

A simplified system to quantify storage of carbon dioxide, water vapor and heat within a maize canopy

Taqi Raza^{1*}, Bruce B Hicks^{1,2}, Joel N. Oetting¹ and Neal S Eash¹

¹Department of Biosystems Engineering and Soil Science, The University of Tennessee, Knoxville USA

²MetCorps, Norris, USA

*Corresponding author: Tagi Raza; taqiraza85@gmail.com, traza@vols.utk.edu

10 Department of Biosystems Engineering and Soil Science, The University of Tennessee, Knoxville
11 USA

Highlights

1. A new multiport system simplifies measuring CO₂ and water vapor gradients in a plant canopy.
2. The system eliminates the effects of sensor calibration differences.
3. Field tests illustrate the ruggedness of the design, suitable for remote and demanding circumstances.
4. Addition of temperature sensors permits application to surface heat storage and energy

for abstract: esp in areas of complex terrain and small plots as confront farming communities in Africa and much of eastern North America

Abstract

23 The canopy storage of CO₂, latent heat and sensible heat within agricultural crops has not yet
24 been fully examined. Reported canopy storage terms are consistently smaller than found for a
25 forest ecosystem, such that they are often neglected. A multiport profile system has been
26 developed to examine these storage terms. The system sequentially samples air from four
27 heights to a single non-dispersive Infrared Gas Analyzer (IRGA). Following extensive laboratory
28 testing, the system has been field proven in an east Tennessee study of a maize crop in 2023.
29 The new system enables quantifications of CO₂ and latent heat atmospheric storage terms and,

30 with supporting temperature measurements, allows improved examination of the surface heat
31 energy budget and the net air-surface exchange of CO₂.

32

33 **Keywords:** Multi-port system, vertical canopy profile, storage terms (CO₂ and heat), energy
34 balance, maize, carbon sequestration

35

36 **1 Introduction**

37 In the last few decades, significant work has attempted to improve our understanding of
38 gaseous exchanges between soils, plants, and the atmosphere. These improvements have been
39 incorporated in land-surface models and numerically-based weather predictions as well as in
40 assessment of atmospheric fluxes of carbon dioxide (Lamas Galdo et al., 2021), water vapor
41 (Wang et al., 2023), and heat over vegetated landscapes (e.g., Hoeltgebaum and Nelson, 2023).

42 Observations of the surface heat budget over forests have shown that the balance
43 expressed by the familiar relationship:

$$44 R_n - G = H + LE \quad (1)$$

45 is not always attained. Here, R_n is net radiation, G is soil heat flux, H is sensible heat flux and LE
46 is latent heat flux (q.v. Wilson et al., 2002). Measurements of the turbulent fluxes H and LE are
47 usually by the eddy covariance (EC) methodology (Nicolini et al., 2018), which is also used to
48 measure the flux of carbon dioxide — F_{CO_2} . In practice, R_n is measured using well-accepted
49 sensors and ground heat flux plates are installed in the soil to determine G . Routine EC
50 measurements are now made at more than 1000 locations globally (c.v. Fluxnet; Pastorello et
51 al., 2020).

52 An important factor emerging from many experimental studies using eddy covariance is
53 that storage terms contribute substantially to energy closure of vegetated areas and to the
54 quantification of evapotranspiration (McCaughy and Saxton, 1988; Hoeltgebaum and Nelson,
55 2023). In concept, errors in the surface heat balance can be attributed to many additional
56 factors, including omission of the heat used in photosynthesis and the storage of heat in plant

57 biomass, in the air below the height of micrometeorological flux measurement and in the soil
58 layer above the depth of G measurement. If the site in question is not flat, horizontal and
59 homogeneous for a considerable distance upwind, then gravity flows, and advection must be
60 expected to play a role. Investigation of these various contributing factors requires
61 measurement of the relevant variables as they change with space and with time; especially
62 challenging due to temporal (particularly diurnal) changes in air temperature and humidity
63 (Varmaghani et al., 2016) as well as in concentrations of carbon dioxide (herein represented by
64 $[CO_2]$).

65 There are several other possible reasons for energy closure errors in EC
66 experimentation, such as loss of low- or high-frequency flux components, non-optimal
67 coordinate rotation, and the use of inappropriate averaging times (Massman and Lee, 2002;
68 Meyers and Hollinger, 2004; Oetting et al., 2024). Finnigan (2006) reported that the
69 atmospheric heat storage term is underestimated when the average sampling time is large.
70 Neglecting canopy storage terms in studies of Net Ecosystem Exchange (NEE) can also cause
71 substantial errors (Raza et al., 2023). Fewer than 30% of known experimental locations apply a
72 profile measurement system to calculate the temporal variations in storage terms (Papale,
73 2006). Many studies report that energy balance closure is an unsolved problem for a variety of
74 vegetation types: the sum of sensible and latent heat flux is found to be 10-30% lower than the
75 available energy (Wilson et al., 2002; Twine et al., 2000; Leuning et al. 2012; Russell et al. 2015;
76 Raza et al., 2023).

77 In the case of agricultural cropping systems, atmospheric storage terms are usually
78 considered small and are often ignored (Nicolini et al., 2018; Raza et al., 2024). Assessments of
79 storage terms within agricultural ecosystems are few and differ from those well documented by
80 researchers in the case of forest ecosystems studies (Mayocchi and Bristow, 1995; Wilson et al.,
81 2002; Hicks et al., 2020). Most results of heat storage in forest environments focus on the
82 atmospheric component of the total heat storage.

83 The present paper focusses on a resolution to needs for detailed measurement of
84 profiles of water vapor and carbon dioxide concentrations in the atmospheric surface

85 roughness layer, as arose in the decade-long sequence of field studies conducted by the dates
86 University of Tennessee in Lesotho, Zimbabwe, Ohio and Tennessee (see Eash et al, O'Dell et al;
87 Hicks et al.). The surface roughness layer is that layer of air in contact with the surface below
88 the height at which familiar micrometeorological flux/gradient relationships apply. These
89 studies have concentrated on aspects of the surface energy balance and crop carbon dioxide
90 exchange in areas different from conventional agricultural-meteorology experiments, namely in
91 areas of complex terrain and small plots as confront farming communities in Africa and much of
92 eastern North America. These experiments have increasingly indicated the importance of
93 detailed temperature and concentration measurements in the surface roughness layer.

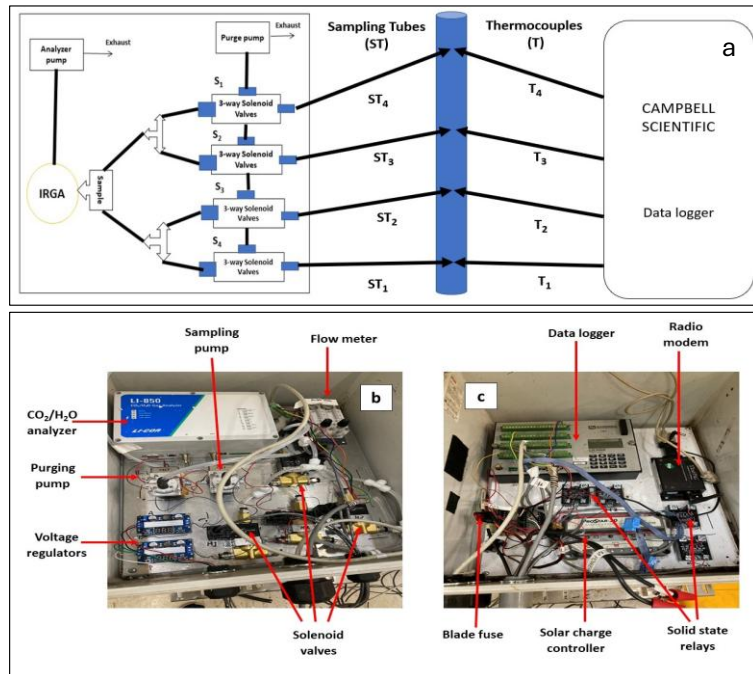
94 A central requirement has been the need to describe water vapor and CO₂
95 concentrations in more detail than conventional micrometeorology normally provides. To this
96 end, the present paper describes an experimental procedure that builds upon air-sampling
97 systems of the past but is streamlined to provide the requisite measurements with the desired
98 time and space detail, in areas often distant from immediate technical support. Some
99 illustrations of its field utility are provided, using observations from a study of a maize canopy in
100 eastern Tennessee in 2023.

101 **2. Apparatus design and operation**

102 The development described here is an outgrowth of experience with eight preceding field
103 studies, conducted at locations in Lesotho, Zimbabwe, Tennessee, and Ohio (Eash et al., 2013;
104 O'Dell et al., 2014, 2015; Hicks et al., 2021, 2022). These demonstrated the need for a reliable
105 yet technically simple system to measure gas concentrations within and above a growing crop.
106 To satisfy the basic requirements for time continuity and reliability of the data record, a new
107 multi-port sampling system was developed.

108 To avoid consequences of individual sensor offsets when gradients are computed, the
109 new system is designed to use a single detection system, in this case an infrared CO₂/H₂O gas
110 analyzer (IRGA; LI-COR-850, Lincoln, NE). Figure 1 presents a schematic description of the
111 apparatus. The system is designed to maintain continuous airflow through all intake tubes, to

112 cycle through all heights of measurement in one minute (7.5 seconds for each height) and to
 113 minimize the switching time between samplings. The system uses two small pumps [Model TD-
 114 3LSA, Brailsford & CO., Inc. Antrium. NH, USA], one pump (the purge pump) draws in air at a
 115 constant rate through all intake tubes to minimize hygroscopic interactions along the tube
 116 walls. Another pump (the sampling pump) pushes the drawn air to the IRGA. The sampling
 117 pump is mounted close to the IRGA so that air smoothly enters the IRGA at ambient pressure.
 118 When sampling the airflow through a specific tube the flow rate is maintained at 1000 ml min^{-1} .
 119 The flow rates through the other three tubes are then maintained at 700 ml min^{-1} by flow
 120 meters [LZQ-7 flowmeter, 101.3 KPa, Hilitland, China]. The switching between sampling tubes is
 121 controlled by four three-way brass and stainless-steel solenoid valves [231Y-6, Ronkonkoma,
 122 NY, USA].



123

124 Fig. 1. Details of the multi-port sampling system: (a) schematic diagram of the manifold for
 125 profile sampling of CO₂ and H₂O, (b) a photograph of the analyzer, pump, and manifold
 126 system, (c) the data logger for data collection.

127 Each sampling tube is same length (10.5 m), to ensure samples from each sampling
 128 height have the same transit time. The purge pump manifold and all sampling tubes are

129 constructed of the same kind of urethane [BEV-A-LINE, Polyethylene material, Cole Parmer,
130 City, State]. Before entering the analyzer, the air is passed through a 1- μ m pore filter [LI-6262,
131 LI-COR, Lincoln NE, USA] to avoid the accumulation of debris, dirt, particles, etc., that can cause
132 contamination in the analyzer optical cells. The air outlet of the purge pump and IRGA are open
133 directly to the atmosphere. Digitizing is at 5 Hz frequency. The data system is arranged to
134 record averages and standard deviations at a pre-arranged periodicity, depending on the
135 research goal but typically 5, 10 or 15 minutes.

136 The performance of the system for measurement of CO₂ and H₂O profiles was examined
137 extensively before its field deployment. The apparatus was first flushed with nitrogen (N₂) gas
138 to create a zero-carbon dioxide environment. Subsequently, a known concentration of CO₂ (430
139 ppm) at ambient pressure was fed through the intake tubes sequentially and system outputs
140 were measured. This process allowed determination of the time taken to reach stable
141 measurement readings.

142 To derive a continuous record of concentrations at each height of interest (in the
143 preliminary configuration, four of them) switching between heights was set at every 7.5
144 seconds allowing each of the heights to be sampled twice in every minute. The laboratory tests
145 showed that after the IRGA received a step change in CO₂ concentration it took approximately
146 1.8 seconds to achieve a steady output. During the laboratory evaluation period, the recorded
147 error was less than 0.5% in [CO₂] between sampling heights. An accuracy error of less than 1%
148 is well within the acceptable range for the IRGA now used according to the specifications
149 provided by the manufacturer and much less than higher errors common in measurements of
150 this kind (Montagnani et al. 2018)

151 **3. Field evaluation**

152 An ongoing field study of a maize crop in East Tennessee provided an opportunity to test the
153 new sampling system in experimentally demanding circumstances. The experiment was at a 23
154 ha plot of agricultural farmland, near Philadelphia, in Loudon County Tennessee (35.673° N,
155 84.465° W). The site is typical of agricultural land used for mainly maize and soybean

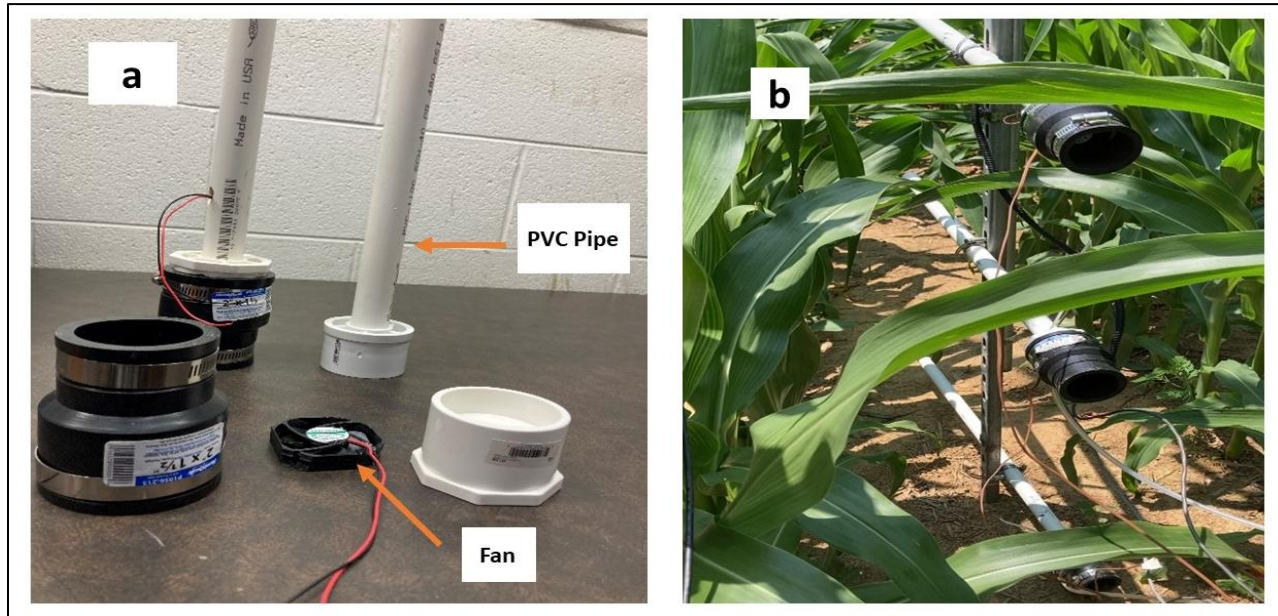
156 production, in slightly rolling terrain that presents a challenge to EC measurements, with local
157 slope varying from 1% to 5% depending on location. For the present purpose, it is not necessary
158 to provide details of the experiment or of the analysis resulting from it. Such detailed
159 examination of the observations will be presented elsewhere. However, the maize variety was
160 "Dekalb 66-06". The mean annual temperature and precipitation of the site are 13.5 °C and 140
161 cm respectively. The soil was classified as an Alcoa Loam (fine, thermic Rhodic Paleudult)
162 according to the USDA-NRCS (2018). The experiment extended through the entire growth cycle,
163 from which data for six weeks during the months of May and June 2023 have been extracted
164 for the present illustrative purpose. Maize planting was on 25 April., so that the illustrations to
165 follow relate to a period of rapid growth of the canopy, from soon after emergence (in early
166 May) to tasseling (in June).

167 In the field test considered here, the system was used to measure at heights of 0.11 m,
168 0.5h, 1+h, 2+h, where h is maize canopy height (in meters) above the soil surface. Note that one
169 intake was permanently set at 0.11 m, and the three other heights were adjusted as the maize
170 grew. Sampling intakes were positioned on a 3.5 m steel mast. Thermocouples at the same
171 height as gas sample intakes were used to measure temperature gradients; these were
172 aspirated within a white PVC pipe shield of 1.9 cm diameter (Figure 2a) that also served as a
173 radiation shield.

174 The experimental program hosting this field test utilized a tripod tower to support an
175 eddy covariance system (adjusted as the crop grew to maintain a height about 2 m above the
176 crown) and supporting micrometeorological measurements — an IRGASON [CO₂/H₂O] open
177 path gas analyzer system, [Campbell Scientific, Logan, Utah], a net radiometer [Kipp & Zonen,
178 OTT HydroMet B.V. Delft, Netherlands], infrared radiometers [IRs-S1-111-SS, Apogee
179 Instruments Inc, City, State, USA], and type T thermocouples [Omega, City, State, USA]. The
180 entire observing system was visually inspected every week for signs of leakage, condensation,
181 and contamination. The IRGASON gas analyzer used for eddy covariance was independent of
182 the IRGA used for concentration gradient measurements. The availability of the EC system and

183 its supporting measurements enabled the tests of the new sampling system to extend to
184 investigation of such matters as the height of origin of thermal eddies, as will be reported later.

185



186

187 Fig. 2. (a) Installation components at each height of the new profile system, showing the
188 aspirated CO₂ intake tubes and thermocouples. (b) Deployment in a maize canopy; the two
189 lowest heights are shown.

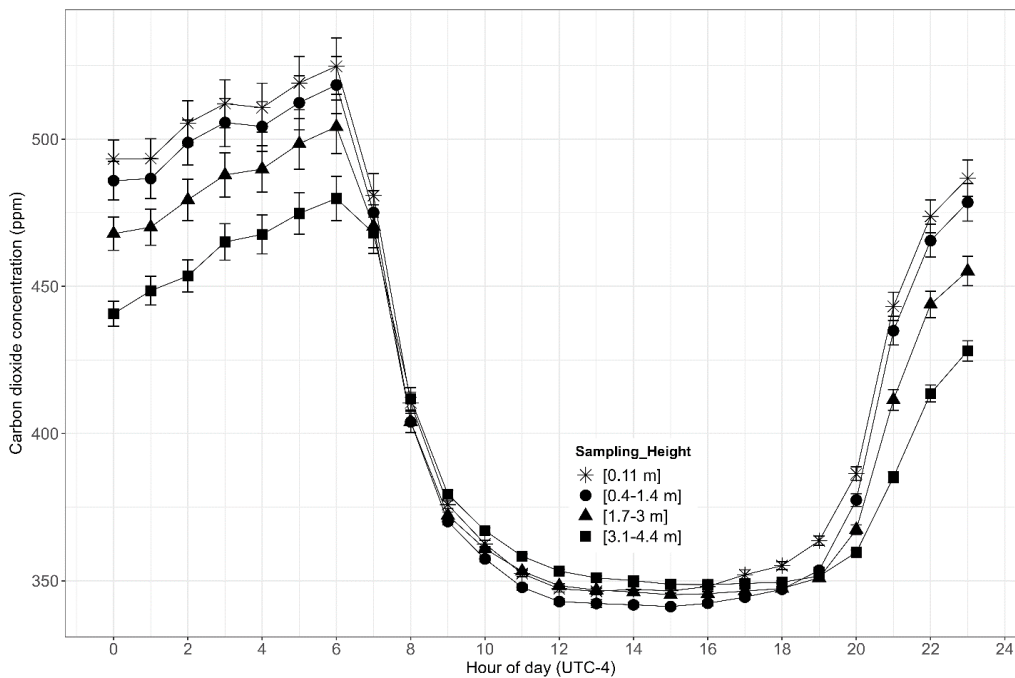
190 3.1. Results — CO₂

191 Within a nocturnal strongly stratified surface roughness layer, previous experiments have
192 revealed the ubiquity of pooling of CO₂ emitted by soil biota and root respiration. Fig. 3
193 presents average diurnal cycles of CO₂ concentrations measured over the six weeks from 18
194 May to 29 June at four heights, two within the canopy and two above. Error bounds correspond
195 to +/- one standard error of the mean. The variability of CO₂ was found to be higher at
196 nighttime than in daytime. The greatest variability was recorded within the canopy, at height 1
197 (0.11 m) and height 2 (0.4 – 1.4 m).

198 The observations confirm the generally accepted features of nocturnal accumulation of
199 CO₂ effluxes from the soil but with detail sufficient to warrant detailed examination. The close

200 tracking of the records for the different measurement heights provides confidence in the
201 performance of the sampling system and indicates that the same causative mechanisms affect
202 all of the heights similarly. The nighttime results that are plotted support the assumptions
203 made elsewhere that changes in the surface stratified atmosphere are mostly in accord with
204 expectations of CO₂ profile linearity (Galmiche and Hunt, 2002; Verma and Rosenberg, 1976), a
205 result that is supported by close examination of CO₂ averages over shorter nighttime periods.

206



207

208 Fig. 3. Average diurnal cycle of CO₂ obtained using the new system described here, for
209 the six weeks. Symbols correspond to different heights of measurements with error bars
210 corresponding to +/- one standard error.

211 Following 0600 local time, about the average time of sunrise, the average
212 concentrations of CO₂ dropped rapidly as photosynthesis commenced and as convection
213 started to mix surface air with the overlying atmosphere. At all heights this initial decrease was
214 followed by a more rapid loss rate until concentrations dropped to about 350 ppm in the
215 afternoon (1200 to 1800 LT), much lower than ambient concentrations thereby reflecting the
216 efficiency with which the maize crop extracted CO₂ from the air. Near sunset, [CO₂] started to

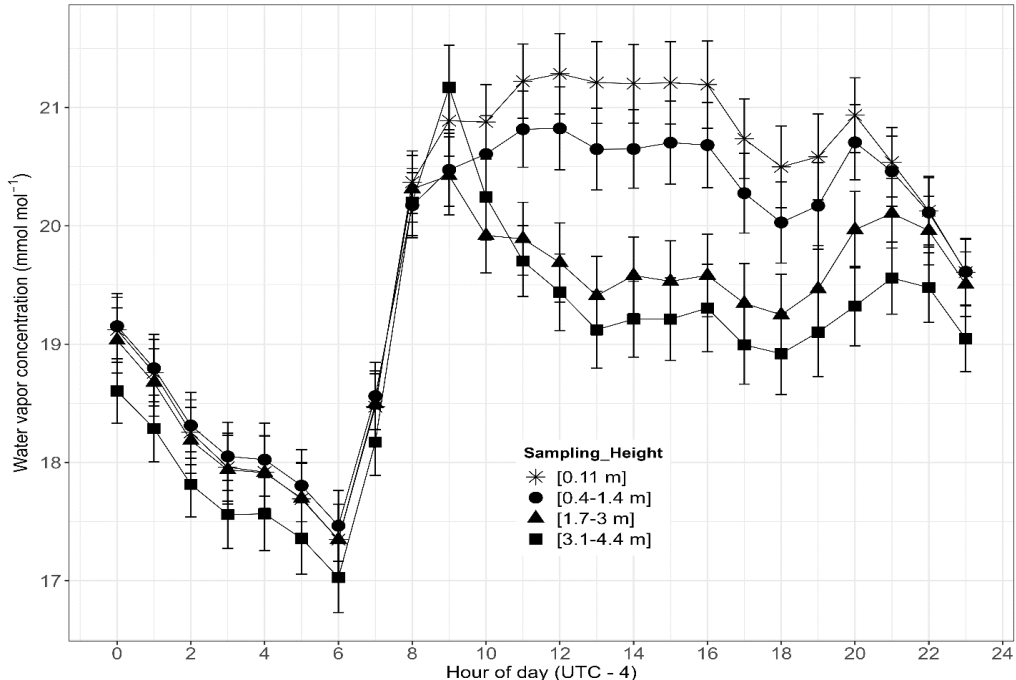
217 increase and continued to build until reaching maximum values immediately before dawn.
218 Concentrations within the canopy do not differ significantly, although the 0.11 m height values
219 always exceed those further above the soil surface. In general, $[\text{CO}_2]$ decreased with increasing
220 height. All of these observations align well with contemporary views of the post-sunrise
221 initiation of photosynthesis and its continuation through the following daylight hours.

222 The nocturnal accumulation of CO_2 observed here is not unusual. In many climatic
223 regions, nighttime soil temperatures remain high enough to sustain microbial and soil
224 respiration activities, resulting in CO_2 accumulation in the stratified air above the ground. After
225 the sun rises, increased light availability increases stomatal activity and photosynthesis rates.

226 **3.2. Results — H_2O**

227 As in Fig. 3, Fig. 4 shows the average diurnal cycle constructed from 15-minute H_2O
228 concentration observations. At all heights a sharp increase in $[\text{H}_2\text{O}]$ was recorded in the
229 morning at the same time as the sudden decrease for $[\text{CO}_2]$ seen in Fig. 3. Subsequently, $[\text{H}_2\text{O}]$
230 peaked at about 0900 LT and, within the canopy, maintained this concentration throughout the
231 daylight hours. Above the canopy average concentrations decreased and a different
232 concentration constancy was attained. After the period around sunset had passed, at about
233 2000 LT, $[\text{H}_2\text{O}]$ started decreasing approximately linearly with time until sunrise approached.
234 The H_2O concentration generally decreased as the measurement height increased for both day
235 and night because a constant source of water vapor was the soil surface, with crop
236 evapotranspiration adding H_2O in the daytime. Dewfall is expected to be important, a
237 contribution that can be uniquely addressed using the new sampling system.
put figures closer to first call-out

238 Figures 4 and 5 reveal considerably different cycles of CO_2 and H_2O . At night, Fig. 3
239 shows a more striking $[\text{CO}_2]$ gradient than does Fig. 4 for $[\text{H}_2\text{O}]$. The reason is presumed to be
240 that CO_2 continues to be emitted from the soil at night and accumulates within the stratified
241 layer of air, whereas there is no parallel process influencing H_2O concentrations. In daytime,
242 there is little consistent $[\text{CO}_2]$ gradient information derivable from Fig. 3, but for $[\text{H}_2\text{O}]$ in Fig. 4
243 there is a clearly visible $[\text{H}_2\text{O}]$ gradient structure. This suggests a slow-down of CO_2 exchange in
244 the afternoons while evaporation continued.



245

246

247 Fig. 4. Average diurnal cycle of the vertical profile of water vapor concentration
 248 averaged over six weeks as in Figs. 3. Symbols correspond to different heights of
 249 measurements with error bars corresponding to +/- one standard error.

250 The processes of evaporation from the soil surface and evapotranspiration from leaves are
 251 linked with solar radiation. Overall, the present results highlight changes in the vertical
 252 distribution of water vapor and its temporal variability, indicating near simultaneity of changes
 253 on CO₂ and H₂O concentrations following dawn (compare Figs. 3 and 4).

254 **Results — atmospheric storage**

255 The vertical profile data can also be used to explore how various atmospheric storage fluxes
 256 influence the CO₂ status and energy budget of the maize crop. In accordance with many
 257 studies of the surface energy budget using EC systems, atmospheric storage terms refer to
 258 depletion or accumulation of scalar quantities (CO₂, H₂O, etc.) in a hypothetical control volume
 259 beneath the height of turbulent flux measurement by EC. A storage flux is defined as the rate
 260 of change of dry molar concentrations of the same variables within the same control volume.
 261 Both concepts relate most directly to the conditions of “perfect” micrometeorology. In

262 practice, natural complexities of surroundings and exposures interfere to the extent that
263 measurements will be site-specific. Moreover, the covariances are statistical quantities, with
264 well-recognized error margins associated with every quantification of them. During this study,
265 the storage fluxes of scalar quantities (CO₂, water vapor, etc.) were calculated using the ICOS
266 methodology (Montagnani et al., 2018). For the case of CO₂,

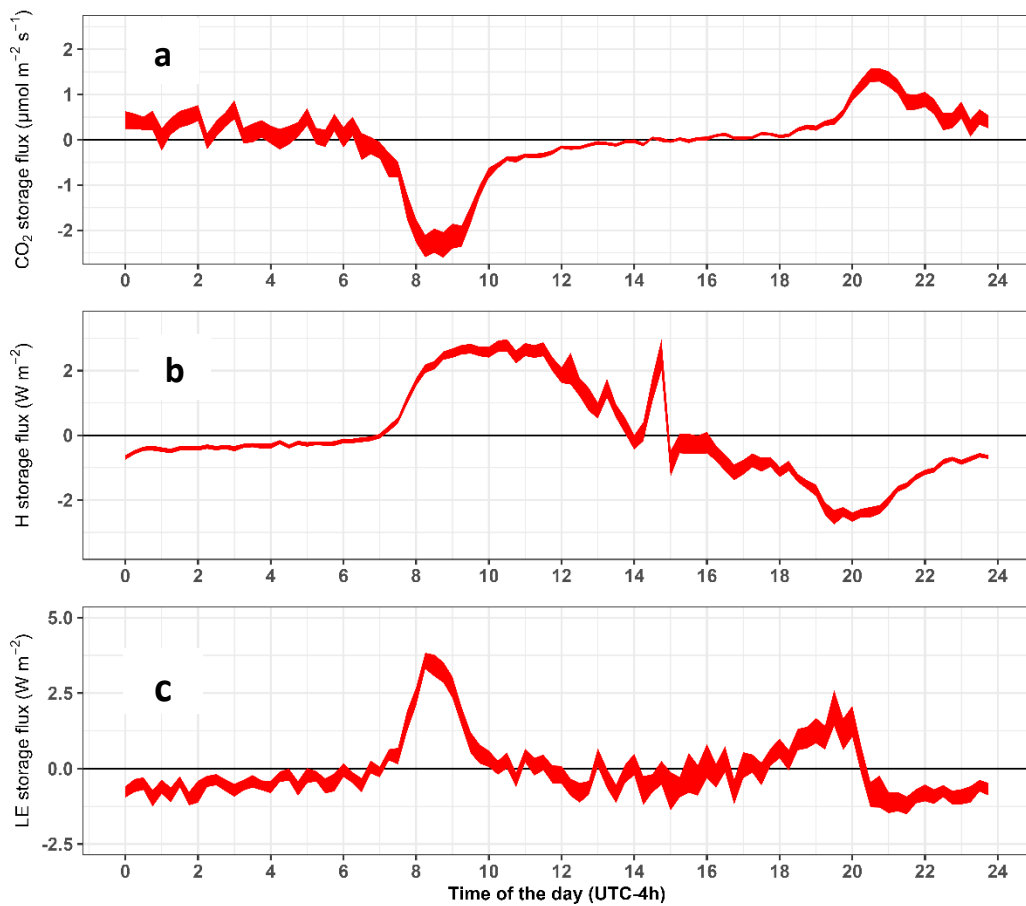
$$267 \quad J_c = \bar{\rho_d} \sum_{i=1}^N \left(\frac{\Delta c}{\Delta t} \right)_i \Delta z_i \quad (2)$$

269

270 Here, J_c is the storage term of CO₂ (for example) within the i_{th} layer over which Δc is measured,
271 Δz_i is the thickness of this layer and Δt is the measurement time step; $\bar{\rho_d}$ is dry air density, and
272 N is the number of layers (number of measurements points). To calculate the storage terms as
273 described by Eq. 2, raw data were averaged into 15-minute periods, yielding the results plotted
274 in Fig. 5. CO₂ storage (Fig. 5a) exhibited a larger magnitude and more variation at nighttime
275 compared to daytime, due to the CO₂ pooling and the intermittency of incursions from air aloft.
276 During the night, photosynthesis did not occur, and CO₂ emitted from the soil accumulated in
277 the overlying stratified atmosphere (Ryan and Law, 2005; Davidson and Janssens, 2006). Soon
278 after sunrise, the nighttime stratification began to weaken, and photosynthesis commenced.
279 The trapped CO₂ was consumed by photosynthesis and mixed with air above the canopy as
280 unstable stratification evolved. Minimal CO₂ storage during the daytime can be due to the
281 instability and strong mixing then prevailing, as well as to the photosynthetic removal of CO₂
282 from the air to which the vegetation was exposed. More efficient exchange between plant and
283 atmosphere then results in low storage of CO₂ in the air space below the uppermost height of
284 [CO₂] measurement. At night, subcanopy ventilation by intermittent gusting results in a large
285 variation between negative and positive CO₂ storage.

286 Observations such as these are facilitated by the profile sampling system now
287 advocated. In the future, it is planned to use the new capability to revisit the quality assurance
288 methodology of EC determinations by comparing atmospheric storage to the statistical
289 uncertainty of the covariances. In this context, note that Fig. 5b indicates sensible heat

290 atmospheric storage terms equivalent, on average, to about 2 W m^{-2} in the late morning,
 291 followed by a downward trend through the afternoon until reaching a minimum a few hours
 292 after sunset. The irregularity seen soon after noon is presently unexplained. Clearly, individual
 293 shorter-term averages could display greater averages and increased scatter, but this remains to
 294 be explored. In comparison, Finkelstein and Sims (2001) derive uncertainties associated with
 295 30-min EC evaluations of the sensible heat covariance in the range 5% to 10% in daytime.



296

297 Fig. 5. Diurnal patterns of CO₂ atmospheric storage (a), sensible heat storage (b) and
 298 latent heat storage (c) of the maize crop in early stages of growth (see Table 1 a-b). The
 299 widths of the traces correspond to +/- one standard error on the means.

300 The nocturnal sensible (Fig. 5b) and latent (5c) heat energy storages remained low and
 301 slightly negative until sunrise, about 0600 LT. As the air cooled during the night, sensible heat
 302 storage in the air mass remained slightly negative as its temperature decreased. After sunrise,

303 the air mass warmed and the sensible heat storage rose to a maximum value of about 2 W m^{-2}
304 between 1200 LT and 1230 LT. Afterwards, the sensible heat storage rate declined, reaching
305 negative values a few hours before sunset and attaining a minimum value (about -1.5 W m^{-2}) a
306 few hours before midnight. The sensible heat storage subsequently trended to near-zero
307 constancy until being disrupted by sunrise at about 0700 LT.

308 Latent heat storage (Fig. 5c) fluctuated near zero for most of the daylight hours, after
309 exhibiting a major positive excursion ($> 4 \text{ W m}^{-2}$) during the few hours after sunrise. After about
310 2100 LT, latent heat storage fluctuations like the variations seen in Fig. 5a occurred until
311 sunrise, with an average of about -0.5 W m^{-2} . Comparison with Fig. 5a indicates that the post-
312 sunrise increases in latent heat storage coincided with the decrease in CO_2 storage. The
313 sensible heat storage appears to have been delayed by a fraction of an hour. Interpretation of
314 these observations requires consideration of dewfall and its evaporation.

315 Table 1 a-b lists some of the plant growth characteristics during the six-weeks
316 considered here. Also listed are the magnitudes of maximum and minimum storage terms
317 during each of the sampling periods, shown here to exemplify the ability of the new sampling
318 system to reveal such extremes. Detailed examination of the plant-atmosphere interaction for
319 the entire growing season will be presented elsewhere. During the six-week evaluation period,
320 CO_2 atmospheric storage increased as the plant grew and as the soil warmed (increasing
321 heterotrophic CO_2 generation, subsurface) but not substantially; the highest storage rate was
322 found at the VT (tasseling) stage and the minimum at the V2 growth stage, five weeks earlier.
323 Similarly, latent heat storage increased significantly, presumably due to increasing leaf area and
324 transpiration. Latent and sensible heat storage was found higher in the VT growth stage than in
325 other growth stages. As the crop grew, different processes became prominent causes of the
326 storage of energy and CO_2 . When the maize was in its early growth stage, the canopy was not
327 fully developed, the soil was cooler, and CO_2 storage did not show much change. However,
328 there were substantial variations in the sensible and latent energy storage terms as the crop
329 grew (see Table 1 a-b).

330 **Table 1 a-b.** Height adjustment during the crop growth stage and maximum and minimum
 331 storage terms. V1 is the first leaf emergence, Vn is when the n^{th} leaf fully emerged, and VT is the
 332 tasseling stage. Height 1 (H_1) was kept constant throughout the experiment while the other three
 333 heights (H_2 , H_3 , and H_4) changed as the plants grew. Negative and positive signs represent the
 334 2.5th percentile (minimum) and 97.5th percentile (maximum) quartile values observed during the
 335 different periods.

Table 1 a	Measurement height (m)				Growth stage	Latent heat Storage	Sensible heat storage
Date	H_1	H_2	H_3	H_4		W m^{-2}	W m^{-2}
May 15-May 21	0.11	0.43	0.60	2.00	V2-V3	-15.19 to 6.13	-5.67 to +2.59
May 22-May 28	0.11	0.43	0.60	2.00	V3-V4	-19.45 to +8.16	-5.67 to +3.21
May 29-June 4	0.11	0.43	1.72	3.07	V5-V6	-19.72 to +8.95	-11.65 to +3.74
June 5-June 11	0.11	0.75	2.10	3.12	V6-V7	-19.72 to +9.01	-45.65 to +4.07
June 12-June 18	0.11	0.95	2.50	3.36	V7-V8	-22.72 to +9.36	-45.65 to +3.68
June 19-June 25	0.11	1.27	3.00	4.36	VT	-22.73 to +9.38	-15.33 to + 4.84

336

337

Table 1 b	Measurement height (m)				Growth stage	CO_2 Storage	Average precipitation	Temperature
Date	H_1	H_2	H_3	H_4		$\mu\text{mol m}^{-2} \text{s}^{-1}$	mm	°C
May 15-May 21	0.11	0.43	0.60	2.00	V2-V3	-7.12 to +2.78	0.00	14.90-25.74
May 22-May 28	0.11	0.43	0.60	2.00	V3-V4	-7.12 to +2.87	0.031	14.59-26.63
May 29-June 4	0.11	0.43	1.72	3.07	V5-V6	-9.54 to +2.59	0.007	14.17-28.12
June 5-June 11	0.11	0.75	2.10	3.12	V6-V7	-9.67 to + 2.33	0.165	12.87-29.70
June 12-June 18	0.11	0.95	2.50	3.36	V7-V8	-9.68 to +2.36	0.081	13.41-29.12
June 19-June 25	0.11	1.27	3.00	4.36	VT	-6.23 to +2.57	0.00	19.22-26.46

338

339

340

341 **4. Conclusions**

342 The field evaluation of the multi-port profile system demonstrated its effectiveness in
343 measurement of CO₂ and H₂O concentrations at different heights within the surface roughness
344 layer. The multiple-height profile system aided substantially to understanding CO₂ and H₂O
345 concentration variations and their vertical profiles, thereby facilitating precise assessments of
346 their exchanges, storage, and overall balance within the growing maize ecosystem. The
347 observations reveal that different processes became prominent at different growth stages,
348 which influenced the atmospheric storage of heat energy and gas and the associated fluxes as
349 the canopy developed. An issue remaining to be addressed is that condensation of water in the
350 sampling tubes was sometimes observed; this will affect measurement accuracy and steps to
351 eliminate the problem are presently being reviewed.

352 The 2023 field experience with the new system indicates that canopy data obtained
353 from the vertical profile observations offer potential for many applications in future studies
354 such as evaluation of soil-plant-atmospheric models that rely on the precise estimation of CO₂,
355 heat and water vapor fluxes. Note that the definition of the heat storage used here (as in Eq.
356 (2)) omits warming of the biomass. This omission accounts for the differences between the
357 storage terms now computed and those published previously (e.g., Hicks et al., 2022).

358 The simplicity of the sampling system device contributes to its success — it suffered a
359 few disruptions during the testing period. This new measurement system will be employed in
360 future studies of air-surface exchange when moderated by the presence of a crop and
361 especially when operation in remote locations is required. Measurements made will permit
362 improved quantification of storage terms — atmospheric, biological, in the soil, and all
363 contributing to a better understanding of the surface heat energy balance. Sub-canopy
364 measurements, in particular, will help track how respiration, evaporation, photosynthesis, etc.
365 vary through the depth of the canopy. Such studies will also help to evaluate
366 micrometeorological models, such as those describing the variation of gases, temperature, and
367 water vapor within a canopy. This new device is now being used for the assessment of canopy
368 gas emissions, starting with carbon dioxide but in the future intended to include nitrous oxide.

369 In summary, this new device has the potential to improve our understanding of soil-plant-
370 atmosphere interactions, particularly within the plant canopies.

371 **Author contribution statement**

372 **TR:** Data curation, Formal analysis, Methodology, Visualization, Writing – original draft. **BBH:** Supervision,
373 Methodology, Visualization, Writing – revision and editing. **NSE:** Supervising, Funding acquisition, Project
374 administration, Writing – review & editing. **JNO:** Formal analysis, writing and reviewing.

375 **Funding**

376 This work was supported by DuPont Tate & Lyle Bio Products Company.

377 **Declaration of competing interest**

378 Authors declare no competing interest associated with this submission.

379 **Acknowledgment**

380 This work was supported by the University of Tennessee, Knoxville. The authors thank David R.
381 Smith (Senior Technical Specialist, BESS, UTK), Wesley C. Wright (Senior Research Associate,
382 BESS, UTK), Scott Karas Trucker (Senior Technical Specialist, BESS, UTK) and Josh Watson
383 (Farmer) for their support.

384 **References**

385 Davidson, E., and Janssens, I.: Temperature sensitivity of soil carbon decomposition and feedbacks
386 to climate change. *Nature*, 440, 165–173, <https://doi.org/10.1038/nature04514>, 2006.

387 Eash, N.S., O'Dell, D., Sauer, T.J., Hicks, B.B., Lambert, D.L. and Thierfelder, C.: Real-time carbon
388 sequestration rates on smallholder fields in Southern Africa. Institute of Agriculture,
389 University of Tennessee, Knoxville, TN., 2013.

390 Finkelstein, P.L. and Sims, P.F.: Sampling error in eddy correlation flux measurements. *J.*
391 *Geophys. Res.: Atmospheres*, 106(D4), 3503–3509,
392 <https://doi.org/10.1029/2000JD900731>, 2001.

393 Finnigan, J.: The storage flux in eddy flux calculations, Agric. For. Meteorol., 136(3–4), 108–113,
394 <https://doi.org/10.1016/j.agrformet.2004.12.010>, 2006.

395 Galmiche, M. and J. C. R. Hunt.: The formation of shear and density layers in stably stratified
396 turbulent flows: linear processes. J. Fluid Mech., 455, 243–262,
397 <https://doi.org/10.1017/S002211200100739X>, 2002.

398 Hicks, B.B., Eash, N.S., O'Dell, D.L. and Oetting, J.N.: Augmented Bowen ratio analysis I: site
399 adequacy, fetch and heat storage (ABRA), Agric. For. Meteorol., 290, 108035,
400 <https://doi.org/10.1016/j.agrformet.2020.108035>, 2020.

401 Hicks, B.B., Lichiheb, N., O'Dell, D.L., Oetting, J.N., Eash, N.S., Heuer, M. and Myles, L.: A
402 statistical approach to surface renewal: The virtual chamber concept. Agrosys. Geosci.
403 Environ., 4(1), p.ee20141, <https://doi.org/10.1002/agg2.20141>, 2021.

404 Hicks, B.B., Oetting, J.N., Eash, N.S. and O'Dell, D.L.: Augmented Bowen ratio analysis, II: Ohio
405 comparisons. Agric. For. Meteorol., 313, 108760,
406 <https://doi.org/10.1016/j.agrformet.2021.108760>, 2022.

407 Hoeltgebaum, L.E.B. and Nelson L.D.: Evaluation of the storage and evapotranspiration terms of
408 the water budget for an agricultural watershed using local and remote-sensing
409 measurements, Agric. For. Meteorol., 341, 109615,
410 <https://doi.org/10.1016/j.agrformet.2023.109615>, 2023.

411 Lamas Galdo, M.I., Rodriguez García, J.D. and Rebollido Lorenzo, J.M.: Numerical model to
412 analyze the physicochemical mechanisms involved in CO₂ absorption by an aqueous
413 ammonia droplet. Int. J. Environ. Res. Public Health, 18(8), p.4119,
414 <https://doi.org/10.3390/ijerph18084119>, 2021.

415 Leuning, R.: Estimation of scalar source/sink distributions in plant canopies using lagrangian
416 dispersion analysis: corrections for atmospheric stability and comparison with a
417 multilayer canopy model, Boundary Layer Meteorol., 96:293–314,
418 <https://doi.org/10.1023/A:1002449700617>, 2012.

419 Massman, W. and Lee, X.: Eddy covariance flux corrections and uncertainties in long-flux
420 studies of carbon and energy exchanges, *Agric. For. Meteorol.*, 113(1–4), 121–144,
421 [https://doi.org/10.1016/S0168-1923\(02\)00105-3](https://doi.org/10.1016/S0168-1923(02)00105-3), 2002.

422 Mayocchi, C.L. and Bristow, K.L.: Soil surface heat flux: some general questions and comments
423 on measurements, *Agric. For. Meteorol.*, 75(1–3), 43–50 (1995).
424 [https://doi.org/10.1016/0168-1923\(94\)02198-S](https://doi.org/10.1016/0168-1923(94)02198-S), 1995.

425 McCaughey, J.H. and Saxton, W.L.: Energy balance storage fluxes in a mixed forest, *Agric. For.*
426 *Meteorol.*, 44(1), 1–18, [https://doi.org/10.1016/0168-1923\(88\)90029-9](https://doi.org/10.1016/0168-1923(88)90029-9), 1988.

427 Meyers, T. P. and Hollinger, S. E.: An assessment of storage terms in the surface energy balance
428 of maize and soybean, *Agric. For. Meteorol.*, 125(1–2), 105–115,
429 <https://doi.org/10.1016/j.agrformet.2004.03.001>, 2004.

430 Montagnani, L., Grünwald, T., Kowalski, A., Mammarella, I., Merbold, L., Metzger, S., Sedlák, P.
431 and Siebicke, L.: Estimating the storage term in eddy covariance measurements: the
432 ICOS methodology, *Int. Agrophysics.*, 32 (4), 551–567, <https://doi: 10.1515/intag-2017-0037>, 2018.

434 Nicolini, G., Aubinet, M., Feigenwinter, C., Heinesch, B., Lindroth, A., Mamadou, O., Moderow,
435 U., Mölder, M., Montagnani, L., Rebmann, C. and Papale, D.: Impact of CO₂ storage flux
436 sampling uncertainty on net ecosystem exchange measured by eddy covariance. *Agri.*
437 *For. Meteorol.*, 248, 228–239, <http://dx.doi.org/10.1016/j.agrformet.2017.09.025>, 2018.

438 O'Dell, D., Sauer, T.J., Hicks, B.B., Thierfelder, C., Lambert, D.M., Logan, J. and Eash, N.S.: A
439 short-term assessment of carbon dioxide fluxes under contrasting agricultural and soil
440 management practices in Zimbabwe. *J. Agri. Sci.* 7(3),
441 <http://dx.doi.org/10.5539/jas.v7n3p32>, 2015.

442 O'Dell, D., Sauer, T.J., Hicks, B.B., Lambert, D.M., Smith, D.R., Bruns, W.A., Basson, A., Marake,
443 M.V., Walker, F., Wilcox, M.D. and Eash, N.S.: Bowen ratio energy balance measurement
444 of carbon dioxide (CO₂) fluxes of no-till and conventional tillage agriculture in Lesotho.
445 Open J. Soil Sci. 4(3): 87–97, <http://hdl.handle.net/10919/70228>, 2014.

446 Oetting, J., Hicks, B. and Eash, N.: On recursive partitioning to refine coordinate rotation in Eddy
447 covariance applications. *Agri. For. Meteorol.*, 1;346:109873,
448 <https://doi.org/10.1016/j.agrformet.2023.109873>, 2024.

449 Papale, D., Reichstein, M., Aubinet, M., Canfora, E., Bernhofer, C., Kutsch, W. and Yakir, D.:
450 Towards a standardized processing of Net Ecosystem Exchange measured with eddy
451 covariance technique: algorithms and uncertainty estimation, *Biogeosci.*, 3(4), 571–583,
452 <https://doi.org/10.5194/bg-3-571-2006>, 2006.

453 Pastorello, G., Trotta, C., Canfora, E., Chu, H., Christianson, D., Cheah, Y.W., Poindexter, C.,
454 Chen, J., Elbashandy, A., Humphrey, M. and Isaac, P.: The FLUXNET2015 dataset and the
455 ONEFlux processing pipeline for eddy covariance data. *Sci. Data*, 7(1), 225,
456 <https://doi.org/10.6084/m9.figshare.12295910>, 2020.

457 Raza, T., Oetting, J., Eash, N., Hicks, B. and Lichiheb, N.: Assessing energy balance closure over
458 maize canopy using multiport system and canopy net storage, in: Proceedings of the
459 104th AMS Annual Meeting, Baltimore, Maryland, USA, 28 January to 1 February, 2024.

460 Raza, T., Hicks, B., Oetting, J. and Eash, N.: On the agricultural eddy covariance storage term:
461 measuring carbon dioxide concentrations and energy exchange inside a maize canopy,
462 in: Proceedings of the 103rd AMS Annual Meeting, Denver, Colorado, USA, 8–12
463 January, 2023.

464 Russell, E.S., Liu, H., Gao, Z., Finn, D. and Lamb, B., Impacts of soil heat flux calculation methods
465 on the surface energy balance closure. *Agricultural and Forest Meteorology*, 214, 189–
466 200, <https://doi.org/10.1038/nature04514>, 2015.

467 Ryan, M., Law, B. Interpreting, measuring, and modeling soil respiration. *Biogeochemistry* 73,
468 3–27, <https://doi.org/10.1007/s10533-004-5167-7>, 2005.

469 Twine, T.E., Kustas, W.P., Norman, J.M., Cook, D.R., Houser, P.R., Meyers, T.P., Prueger, J.H.,
470 Starks, P.J. and Wesely, M.L.: Correcting eddy-covariance flux underestimates over a

471 grassland, Agric. For. Meteorol., 103 (3), 279–300, [https://doi.org/10.1016/S0168-1923\(00\)00123-4](https://doi.org/10.1016/S0168-1923(00)00123-4), 2000.

473 USDA-NRCS (2018). Soil Survey Staff, Natural Resources Conservation Service, United States
474 Department of Agriculture. Web Soil Survey. Available at:
475 <https://websoilsurvey.sc.egov.usda.gov/App/WebSoilSurvey.aspx>, Accessed November
476 2018.

477 Varmaghani, A., Eichinger, W.E. and Prueger, J.H.: A diagnostic approach towards the causes of
478 energy balance closure problem. Open J. Mod. Hydrol., 6(02), 101,
479 <https://doi.org/10.4236/ojmh.2016.62009>, 2016.

480 Verma, S.B. and Rosenberg, N.J.: Vertical profiles of carbon dioxide concentration in stable
481 stratification. Agric. Meteorol, 16(3), 359–369, [https://doi.org/10.1016/0002-1571\(76\)90005-4](https://doi.org/10.1016/0002-1571(76)90005-4), 1976.

483 Wang, X., Zhong, L., Ma, Y., Fu, Y., Han, C., Li, P., Wang, Z. and Qi, Y.: Estimation of hourly actual
484 evapotranspiration over the Tibetan Plateau from multi-source data. Atmos. Res., 281,
485 106475, <https://doi.org/10.1016/j.atmosres.2022.106475>, 2023.

486 Wilson, K.B., Goldstein, A., Falge, E., Aubinet, M., Baldocchi, D., Berbigier, P., Bernhofer, C.,
487 Ceulemans, R., Dolman, H., Field, C., Grelle, A., Ibrom, A., Law, B., Kowalski, A., Meyers,
488 T., Moncrieff, J., Monson, R., Oechal, W., Tenhunen, J., Valentini, R. and Verma, S.:
489 Energy balance closure at FLUXNET sites, Agric. For. Meteorol., 113, 223–243,
490 [https://doi.org/10.1016/S0168-1923\(02\)00109-0](https://doi.org/10.1016/S0168-1923(02)00109-0), 2002.